Journal of Electrical Engineering & Technology Vol. 6, No. 4, pp. 447~458, 2011 **447**
DOI: 10.5370/JEET.2011.6.4.447

A Novel Energy Storage System based on Flywheel for Improving Power System Stability

Jinbo Wu†, Jinyu Wen*, Haishun Sun* and Shijie Cheng*

Abstract – In this paper, a novel flywheel energy storage device, called the flexible power conditioner, which integrates both the characteristics of the flywheel energy storage and the doubly-fed induction machine, is proposed to improve power system stability. A prototype is developed and its principle, composition, and design are described in detail. The control system is investigated and the operating characteristics are analyzed. The test results based on the prototype are presented and evaluated. The test results illustrate that the prototype meets the design requirement on power regulation and starting, and provides a cost-effective and effective means to improve power system stability.

Keywords: Flexible power conditioner, Flywheels, Doubly-fed induction machines, Energy storage, Power system stability

1. Introduction

The secure and stable operation of power systems is heavily dependent on the power balance between the generators and the loads. Renewable energy generation changes, load changes or short-circuit faults on the transmission lines, or a variety of power system equipment may cause power imbalance between the supply and demand sides. This power imbalance may become the root cause of power system instability and even blackouts. Using energy storage devices in power systems is a promising means to compensate for the unbalanced power and enhance system stability.

Batteries have been traditionally used to store energy, but their service times are generally too limited to be widely used in power systems 0–4]. Capacitors, including super-capacitors, are frequently used to compensate for power inadequacy in power systems, but they are incapable of supplying active power 0–8]. Flywheel energy storage systems have very high power density and high energy density at high speed. They also have long service times, low maintenance costs, and are insensitive to environmental changes. The concept of using flywheels to store energy has been applied with some amount of success, typically, in wind power generation, automotive, and aerospace applications 0–13]. However, the application of this energy storage method to enhance power system stability is just beginning to be studied 0–15].

This paper proposes a novel energy storage system based on flywheel, called the flexible power conditioner (FPC). As shown in Fig. 1, the FPC is composed of a doubly-fed induction machine (DFIM), a flywheel with very large rotating inertia, a voltage-source pulse width modulation (PWM) rectifier-inverter pair connected between the rotor and the grid and used as an AC exciter, and a corresponding control system.

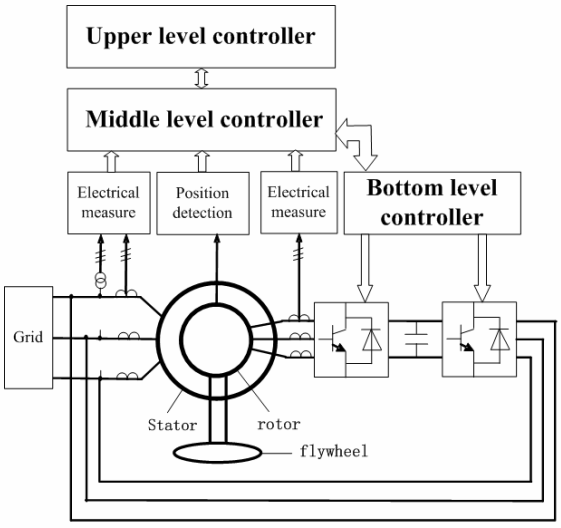

Fig. 1. Structure of the proposed FPC

Traditional flywheel energy storage systems typically use synchronous machines to drive flywheels and are controlled by back-to-back rectifier-inverter pairs. On the other hand, DFIMs, which have been widely used in wind power generation 0–18], are applicable in flywheel drive systems. Compared with the synchronous machine technology, the DFIM approach is more effective due to its ability to deal with large rotor speed variations around the

† Corresponding Author: Department of Science and Technology Huazhong University (jinbowu1112@qq.com)
* Department of Science and Technology Huazhong University
Received: November 19, 2010; Accepted: February 28, 2011

synchronous speed and to achieve full speed-range control of the machine by excitation converters rated at only a fraction of the total power 0–21].

By incorporating the flywheel energy storage and the DFIM, the proposed FPC is able to store energy as available, supply a large amount of active power as needed, and provide reactive power for voltage support as necessary 0–23]. The advantages of the proposed approach are as follows: First, the induction machine can be controlled to work as a generator or as a motor, second, a prime mover is not needed to generate active power. In addition, the classical oriented vector control can be used to control the power converters.

A prototype of the FPC is developed as shown in Fig. 2(a). The rest of the paper is organized as follows: In Section 2, the structure of an FPC based on the flywheel is described. The control system of the prototype is investigated in Section 3. Section 4 analyzes the FPC operating characteristics. The test results of the prototype are presented and evaluated in Section 5.

(a) The FPC prototype

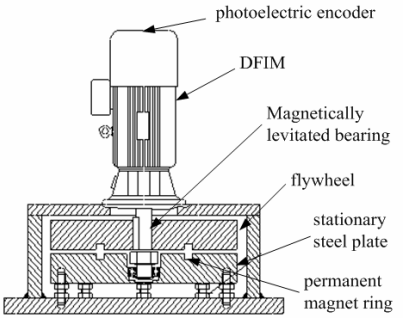

(b) Structure of the flywheel and drive motor

Fig. 2. Structure of the proposed FPC

2. Structure

The structure of the proposed FPC is shown in Fig. 1. The dynamic energy stored in the rotor (or flywheel) is determined by

$$E = J\omega_r^2/2 \tag{1}$$

where J represents the rotor inertia, and ω_r is the rotor electrical angular speed. As the rotational speed is kept constant, the stored energy is proportional to the inertia of the flywheel.

FPC is a novel flywheel energy storage device which integrates both the characteristics of the flywheel energy storage and the DFIM. The structure diagram of the flywheel and drive motor is shown in Fig. 2, where the flywheel with very large rotating inertia is at the bottom and the DFIM is at the top. For storing/releasing energy, the structure of the DFIM is designed as the vertical three-phase wound rotor induction motor and the motor is operated in a no-load and no-turbine-driving condition that is different from the DFIM used in wind power generation. Its stator windings are connected with the power grid, and the rotor windings are connected with the AC excite. In addition, a photoelectric encoder is installed at the top of the DFIM to measure the rotor position, and a flywheel is added to the rotor in order to increase the inertia of the rotor. Magnetically levitated bearing is used to decrease the friction loss of the rotating shaft. To levitate the flywheel, a permanent magnet ring is added at the bottom and a stationary steel plate the same size as the flywheel is fixed under it.

By controlling a pair of back-to-back connected voltage source converters, the change in the rotational speed of the DFIM and the flywheel is achieved; therefore, energy is stored or released. One power converter is connected with the power grid and converts the three-phase grid voltage to a DC voltage. The converter connected with the rotor windings can provide AC excitation currents with the required amplitude, frequency, and phase in which a vector control technology is used 0.

3. Control System

The control system of the FPC is composed of three controllers: upper level controller, middle level controller, and bottom level controller. The upper level controller performs variable sampling operations and coordinates the controls between the FPC and other devices in the system by taking the power system stability analysis into full consideration. It calculates the active and reactive power exchanges between the FPC and the grid for the power system stability. The upper level controller also produces the power set points for the middle level controller. Using a suitable vector control strategy, the middle level controller calculates the three-phase variable-frequency excitation voltages for the rotor excitation of the FPC. The bottom level controller performs the PWM technology-based excitation control, as proposed in 0.

Changing the sinusoid modulation waveforms of the inverter can change the frequency, phase, and magnitude of

the excitation voltage for the DFIM. The rectifier is mainly used to keep the voltage of the capacitor U_{dc} constant. This control technology has been widely used in pumped-storage units and wind-mill generators 0–28]. For simplicity, the detailed design of the bottom level controller is not discussed in detail in this paper.

The DFIM is modeled by the following equations in the direct (d) and quadrature (q) axis reference frame 0, 29], which rotates at synchronous speed ($\omega_1=2\pi f_1$):

$$\begin{cases} u_{sd} = -R_s i_{sd} - \dfrac{\partial \psi_{sd}}{\partial t} + \omega_1 \psi_{sq} \\ u_{sq} = -R_s i_{sq} - \dfrac{\partial \psi_{sq}}{\partial t} - \omega_1 \psi_{sd} \\ u_{rd} = R_r i_{rd} + \dfrac{\partial \psi_{rd}}{\partial t} - \omega_s \psi_{rq} \\ u_{rq} = R_r i_{rq} + \dfrac{\partial \psi_{rq}}{\partial t} + \omega_s \psi_{rd} \end{cases} \tag{2}$$

$$T_e = n_p L_m (i_{sq} i_{rd} - i_{sd} i_{rq}) \tag{3}$$

$$T_m - T_e = -T_e = \frac{J}{n_p}\frac{\partial \omega_r}{\partial t} + \frac{D}{n_p}\omega_r \tag{4}$$

$$\begin{cases} \psi_{sd} = L_s i_{sd} - L_m i_{rd} \\ \psi_{sq} = L_s i_{sq} - L_m i_{rq} \\ \psi_{rd} = L_r i_{rd} - L_m i_{sd} \\ \psi_{rq} = L_r i_{rq} - L_m i_{sq} \end{cases} \tag{5}$$

$$\begin{cases} P_s = u_{sd} i_{sd} + u_{sq} i_{sq} \\ Q_s = u_{sq} i_{sd} - u_{sd} i_{sq} \end{cases} \tag{6}$$

$$\begin{cases} P_r = u_{rd} i_{rd} + u_{rq} i_{rq} \\ Q_r = u_{rq} i_{rd} - u_{rd} i_{rq} \end{cases} \tag{7}$$

where u is the voltage, i is the current, R is the resistance, L is the reactance, Ψ is the flux linkage, T_e represents the electromagnetic torque, and $\omega_1=2\pi f_1$ is the synchronous electrical angular speed. $\omega_s=\omega_1-\omega_r$. P_s and P_r is the stator output active power and rotor input active power, respectively. Subscripts d and q indicate the direct-and quadrature-axis components under the rotation synchronizing reference frame. Subscripts s, r, and m indicate the stator, the rotor, and the mutual quantities, respectively. D represents the damping torque coefficient proportional to the rotor angular speed. n_p is the number of pole-pairs. The mechanical torque T_m is zero.

The stator flux linkage orientation control technology is used to ascertain the excitation voltage of the DFIM used in wind power generation. However, the precise measurement of the flux linkage is difficult to obtain. The voltage is easy to detect and control. The stator voltage orientation control (SVOC) technology is used to design the middle level controller of the FPC as shown in Fig. 3. The SVOC orients the q axis of the synchronous reference frame along the stator voltage and the d axis is 90° behind the q axis.

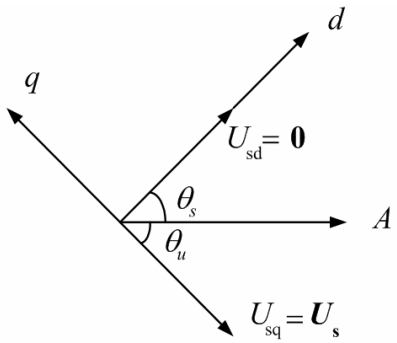

Fig. 3. SVOC technology

By not taking into account the derivatives of the stator and rotor flux and considering R_s, the steady state equations are deduced:

$$\begin{cases} U_{sd} = 0 \\ U_{sq} = U_s \end{cases} \tag{8}$$

$$\begin{cases} \psi_{sq} = \dfrac{R_s i_{sd}}{\omega_1} \\ \psi_{sd} = -\dfrac{U_s + R_s i_{sq}}{\omega_1} \end{cases} \tag{9}$$

$$\begin{cases} P_s = U_s i_{sq} \\ Q_s = U_s i_{sd} \end{cases} \tag{10}$$

$$\begin{cases} U_{rq} = U'_{rq} + U_s \dfrac{\omega_s L_r}{\omega_1 L_m} + \sigma \omega_s I_{sd} \\ U_{rd} = U'_{rd} - \sigma \omega_s I_{sq} \end{cases} \tag{11}$$

where $\sigma = L_s L_r / L_m - L_m$.

The middle level controller is designed to conduct the excitation control by decoupling the control of the active and reactive powers. A small amount of power flow exists between the rotor windings and the grid. The proposed excitation control is designed and aimed at the power flow of the stator windings. The active and reactive power flows of the rotor windings are compensated in the power set points produced by the upper level controller. The middle level controller is composed of the power and current loops, as shown in Figs. 4(a) and (b). P_{ref} and Q_{ref} are the power set points produced by the upper level controller.

The upper level controller implements the control strategy at the power system level. The flexible design of the upper level controller is adopted according to the requirements of power systems. Besides setting P_{ref} and Q_{ref} directly, the upper level controller generates the regulation power signal depending on the grid requirement and FPC current state. In the FPC prototype, variable sampling PI control is used to calculate the active and reactive power exchanges between the FPC and the grid for the power system stability. The developed control strategy

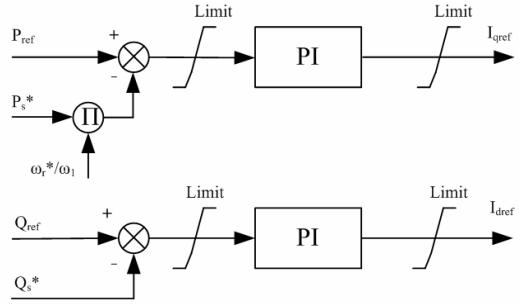

(a) Power loop

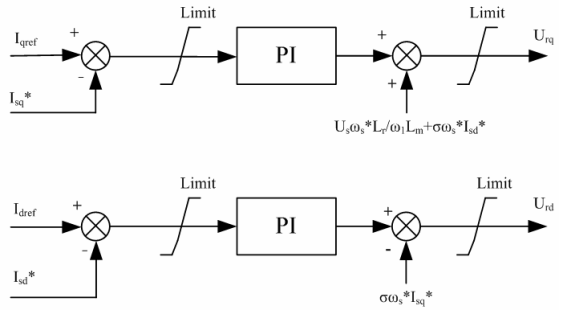

(b) Current loop

Fig. 4. Control diagrams of the middle level controller

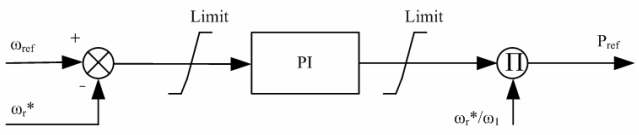

Fig. 5. Control strategy for direct start for P_{ref}

for direct start is used in the monitoring system of the prototype.

With appropriate control, the back-to-back power converter pair can generate a three-phase AC voltage over a wide frequency range around the power system line frequency; thus, it is possible to directly start the FPC. The control strategy for direct start seeks to increase ω_{r} from zero to the set point as smoothly as possible and to reduce the impact on the gird.

As shown in Fig. 5, P_{ref} is obtained by the speed control. The rotor active power is near the stator power because s is near 1 at the starting point. To ensure that the rotor power is not more than the maximum active power, P_{ref} is gradually increased from zero.

At the initial stage of the starting point, the rotor current is small and the reactive power generated by the converter is insufficient to provide the needs for starting the FPC. Absorbing reactive power from the grid is required. Thus, Q_{ref} is evaluated directly by the following:

$$\begin{cases} Q_{ref} = -2kVar & \omega_r \le 250r/\min \\ Q_{ref} = 0 & \omega_r > 250r/\min \end{cases} \tag{12}$$

4. Operating Characteristic Analysis

The power flow between the FPC and the grid is discussed as follows. As shown in Fig. 6, the power flows of the stator-side windings, rotor-side windings, and total are given by the following equations:

$$\begin{cases} P_s = T_e\omega_1 \\ P_r = sP_s = sT_e\omega_1 \\ P = P_s - P_r = (1-s)T_e\omega_1 \end{cases} \tag{13}$$

where P is the total output active power.

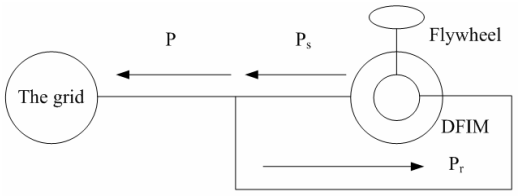

Fig. 6. Diagram of power flow between the FPC and the grid

Compared with the flywheel system which uses the synchronous machine, the FPC which uses the DFIM is more effective due to its ability to control the flywheel system by excitation converters rated at only a fraction of the total power with large flywheel speed variations around the synchronous speed. Fig. 7 shows the simulation comparison result of the FPC with the flywheel system which used the synchronous machine in the output power through the converters in the case of releasing power 4 kW and storing power 4 kW. As shown in Fig. 7, the output power through the converters of the FPC is smaller than that of the flywheel system which used the synchronous machine, especially when ω_{r} variations are from 700 r/min to 1500 r/min. Moreover, ω_{r} variations from 700 r/min to 1500 r/min is the FPC main operation range. Therefore, the FPC which used the DFIM is more cost-effective than the flywheel system which used the synchronous machine.

The two modes of operation in the FPC, namely, sub-synchronous and super-synchronous modes, are calculated by the slip ratio s.

In the sub-synchronous mode (s>0), the rotor speed of the FPC is always lower than the synchronous speed, which means that the slip ratio s>0. Therefore, the direction of the stator active power is opposite to that of the rotor active power. When the stator-side windings of the FPC take energy in from the grid, the rotor-side windings release energy to the grid through the power converter pair. The rotor-side windings store energy as the stator releases energy to the grid. The direction of the total active power is the same as that of the stator active power because the value of the rotor active power is less than that of the stator

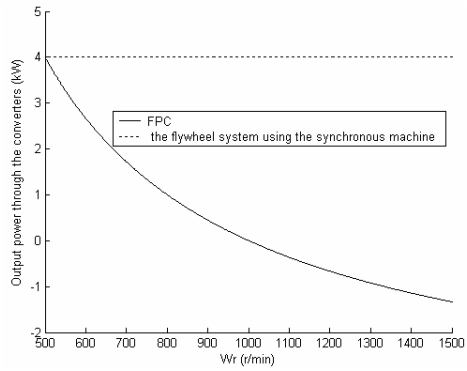

(a) Releasing power 4 kW

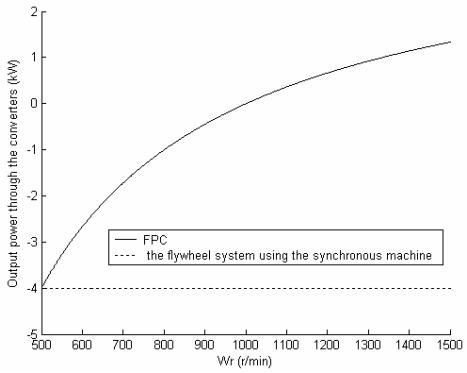

(b) Storing power 4 kW

Fig. 7. Simulation comparison of the FPC with the flywheel system which used the synchronous machine

active power. The value of the total active power is the difference of the stator active power and the rotor active power.

In the super-synchronous mode (s<0), the rotor speed is always higher than the synchronous speed, which means that the slip ratio s<0. Therefore, as the stator-side windings store energy from the grid, the rotor-side windings store energy from the grid. While the stator releases energy to the grid, the rotor releases energy through the power converter pair. The direction of the rotor active power and the stator active power are also the same as that of the total active power. The value of the total active power is the sum of the stator and reactive active power.

Whether the FPC works in the sub-synchronous mode or the super-synchronous mode, it can flexibly regulate reactive power by changing the amplitude of the exciting current as synchronous compensator. The only difference is that, in theory, the FPC is able to work stably at any speed. The rotor speed is computed by the following equation:

$$f_M = \frac{f_1 - f_e}{p} \tag{14}$$

where f_1 represents the synchronous frequency, f_M and f_e indicate the rotor mechanical angular frequency and the exciting current frequency, respectively, and p is the number of pole-pairs.

It is inconvenient for the converters to provide DC excitation currents. In general, the FPC working in synchronous speed can be avoided. The stator side reactive power is exchanged with the grid and the rotor side reactive power is absorbed by the converter.

5. Test Results

The FPC prototype is developed and its corresponding parameters are presented in the Appendix. The control system is designed in Section 3. The relationship of the total output power and the stator and rotor currents are presented by the following equations:

$$\begin{cases} I_{sq} = \dfrac{\omega_1 P}{\omega_r U_s} \\ I_{sd} = \dfrac{Q}{U_s} \end{cases} \tag{15}$$

$$\begin{cases} I_{rq} = \dfrac{\omega_1 L_s P}{\omega_r L_m U_s} + \dfrac{R_r L_s Q}{\omega_s L_m L_r U_s} \\ I_{sd} = \dfrac{U_s}{\omega_1 L_m} + \dfrac{L_s Q}{L_m U_s} - \dfrac{\omega_1 R_r L_s P}{\omega_s \omega_r L_m L_r U_s} \end{cases} \tag{16}$$

As showh in Fig. 8, the prototype is investigated for the power exchange between the prototype and the grid in the laboratory. The grid voltage is set to 380 V. The stator of the DFIM is connected with the grid and the rotor is connected with the converter. The transformer connected between the converter and the grid is used to lower the converter voltage, and the prototype is also able to work at 800 V. The monitoring system of the prototype, as the upper level controller, starts the prototype and sets the points of the exchanged active and reactive powers between the prototype and the grid. The converter, as the middle and bottom level controller, controls the DFIM by changing the excitation current according to the set points from the monitoring system. Figs. 9–13 show the laboratory test results and the test data obtained from the oscilloscope.

5.1 Direct Start

The prototype is tested at direct start. The rectifier cuts in at first, then the inverter cuts in at 2 s when the DC-link voltage has been stabilized. After the inverter cuts in, the proposed control strategy for direct start is used to direct start the prototype. Since the grid voltage is 380 V, the limitation of the active power set points is set to 2 kW to avoid rotor currents that are too big. ω_{ref} can be set at any value within the working range of ω_{r}. Fig. 9 shows the test

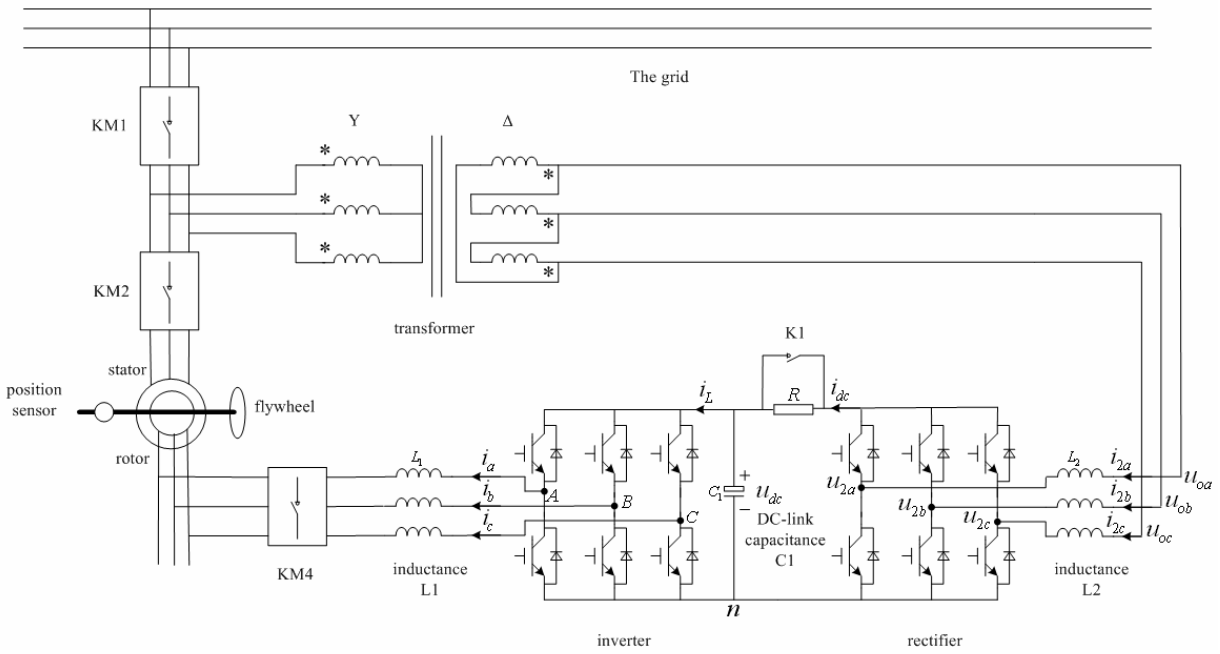

Fig. 8. Diagram of the laboratory experiment

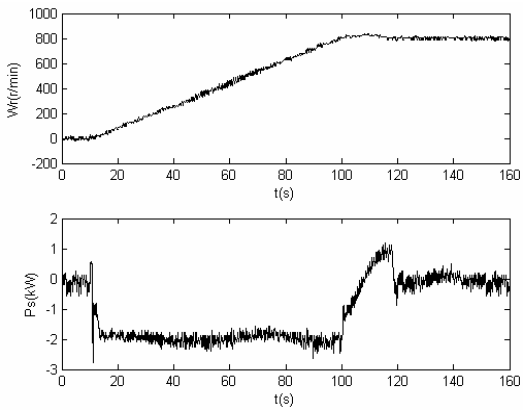

(a) ω_r, P_s

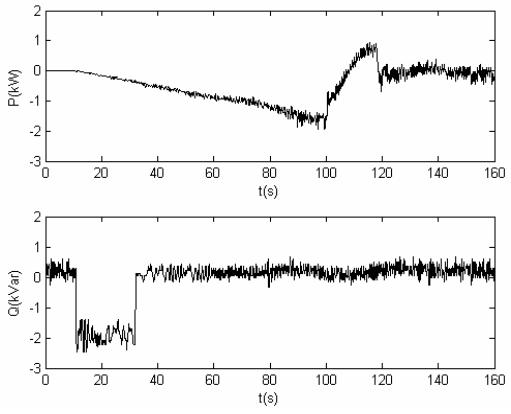

(b) P, Q

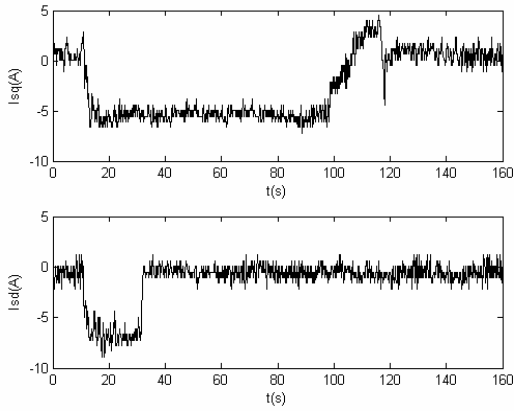

(c) I_{sq}, I_{sd}

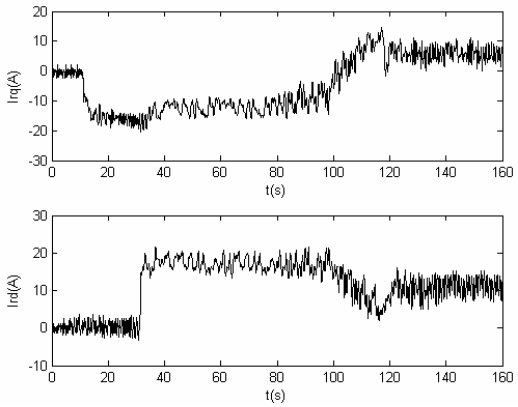

(d) I_{rq}, I_{rd}

Fig. 9. Test results of the prototype at direct start.

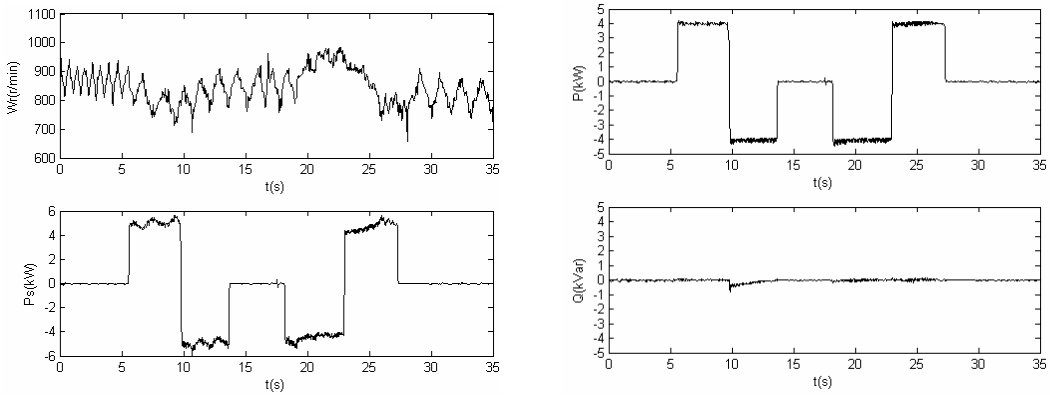

(a) ω_r, P_s (b) P, Q

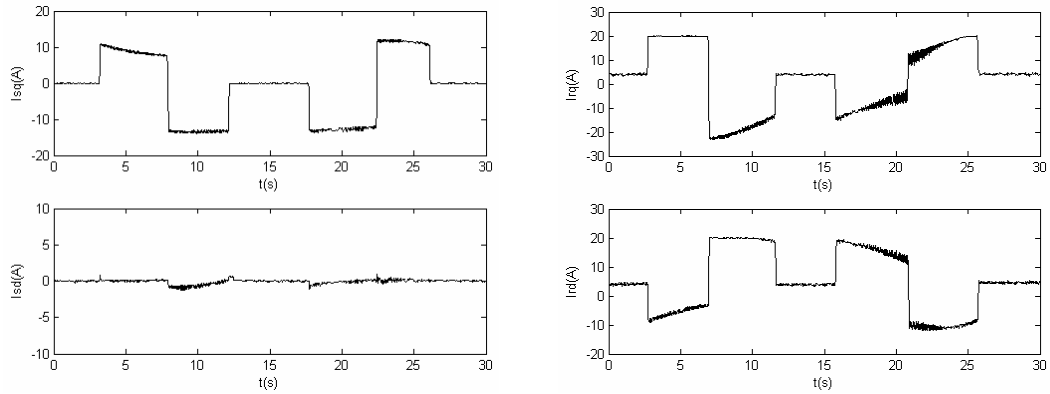

(c) I_{sq}, I_{sd} (d) I_{rq}, I_{rd}

Fig. 10. Test results of the FPC prototype on P regulation at sub-synchronous

results of the prototype at direct start (ω_{ref}=800 r/min).

The prototype is tested at direct start. The rectifier cuts in at first, then the inverter cuts in at 2 s when the DC-link voltage has been stabilized. After the inverter cuts in, the proposed control strategy for direct start is used to direct start the prototype. Since the grid voltage is 380 V, the limitation of the active power set points is set to 2 kW to avoid the rotor currents that are too big. ω_{ref} can be set at any value within the working range of ω_r. Fig. 9 shows the test results of the prototype at direct start (ω_{ref}=800 r/min).

Fig. 9(a)–(d) show the curves of ω_r, P_s, P, Q, I_{sq}, I_{sd}, I_{rq}, and I_{rd} at direct start, respectively. As shown in Fig. 9, the start time of the prototype from 0 to 800 r/min is 110 s. During the direct start, ω_r changes smoothly without acute acceleration and deceleration. The overshoot value of ω_r is about 30 r/min, and the time is about 20 s. P gradually increases from 0 to -1.2 kW, and P_s is maintained at near-2 kW. Their relationship is the same as shown in (13). At the initial stage of the direct start, Q is about -2 kVar and Q changes to zero after ω_r is up to 250 r/min. The process of change in Q is the same as that shown in (16). P and Q are the same as P_{ref} and Q_{ref} obtained by the control algorithm for starting. During the direct start, the change of I_{sq}, I_{sd}, I_{rq}, and I_{rd} are the same as shown from (15) to (16).

5.2 Sub-Synchronous

The prototype is tested on the power regulation at sub-synchronous. P_{ref} and Q_{ref} can be set at any value within the working range of P and Q. Figs. 10–12 show the test results of the prototype on the power regulation at sub-synchronous.

When the prototype is tested on P regulation, the order of the P_{ref} value is 0, 4kW, -4kW, 0, -4kW, 4kW, and 0, and the Q_{ref} value constant is 0. When the prototype is tested on Q regulation, the P_{ref} value is maintained at 0, and the order of the Q_{ref} value is 0, 4kVar, -4kVar, 0, -4kVar, 4kVar, and 0. Figs. 10–11 show the test results of the prototype on P and Q regulations at sub-synchronous, respectively.

Figs. 10–11 show the curves of ω_r, P_s, P, Q, I_{sq}, I_{sd}, I_{rq}, and I_{rd} on P and Q regulations at sub-synchronous, respectively. As shown in Figs. 10–11, the P and Q regulations of the prototype at sub-synchronous are implemented satisfactorily. Satisfactory performances of P and Q are obtained. ω_r accelerates or decelerates with the positive or negative value of P. Due to its loss, ω_r also slows down when P is zero. The relationship between P and P_s is the same as shown in (13). During the power regulation at sub-synchronous, the changes of I_{sq}, I_{sd}, I_{rq},

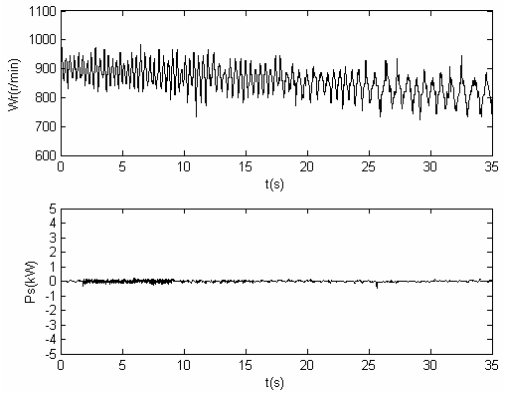

(a) ω_r, P_s

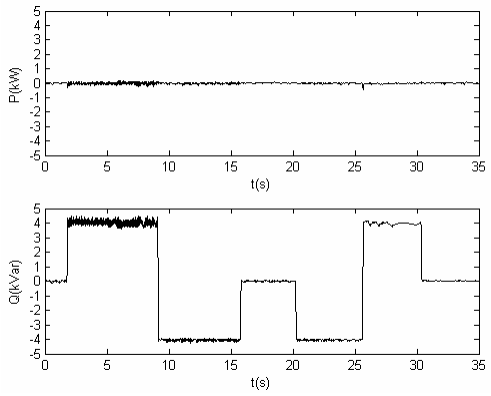

(b) P, Q

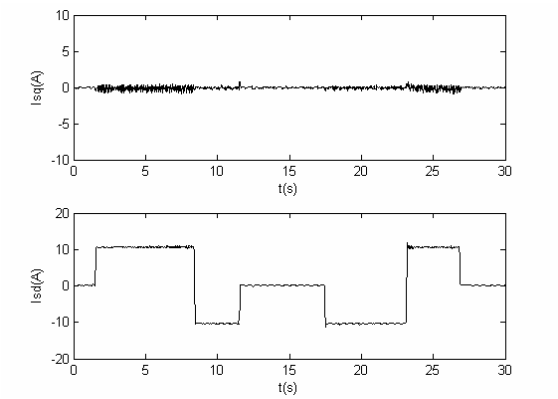

(c) I_{sq}, I_{sd}

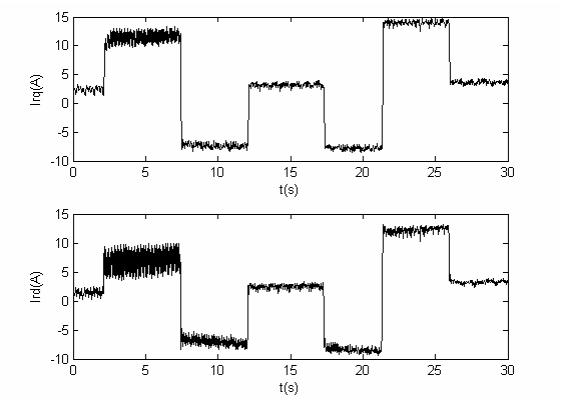

(d) I_{rq}, I_{rd}

Fig. 11. Test results of the FPC prototype on Q regulation at sub-synchronous

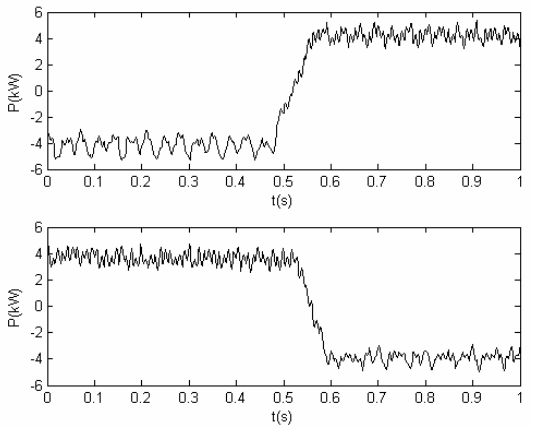

(a) P responses

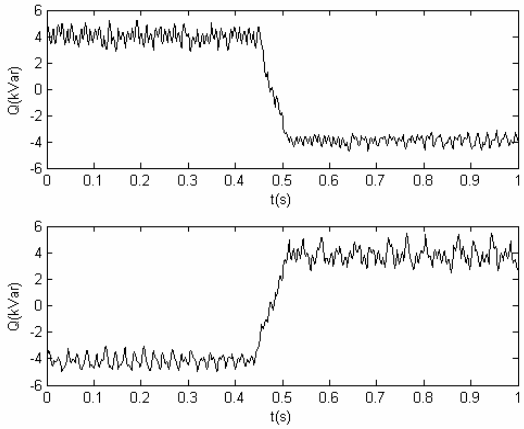

(b) Q responses

Fig. 12. Power dynamic response of FPC prototype at sub-synchronous

and I_{rd} are the same as shown in (15)–(16). In Figs. 10–11, the power regulation at sub-synchronous is implemented satisfactorily.

Fig. 12 shows the power dynamic response of the FPC prototype at sub-synchronous. Fig. 12(a) and (b) show the P and Q responses at sub-synchronous, respectively. In Fig. 12, the P ramp time from -4 kW to 4 kW is 100 ms; the P ramp time from 4 kW to -4 kW is 70 ms; and the Q ramp time from 4 kW to -4 kW and from -4 kW to 4 kW are both about 60 ms. The sensitive response of the power regulation at sub-synchronous is obtained.

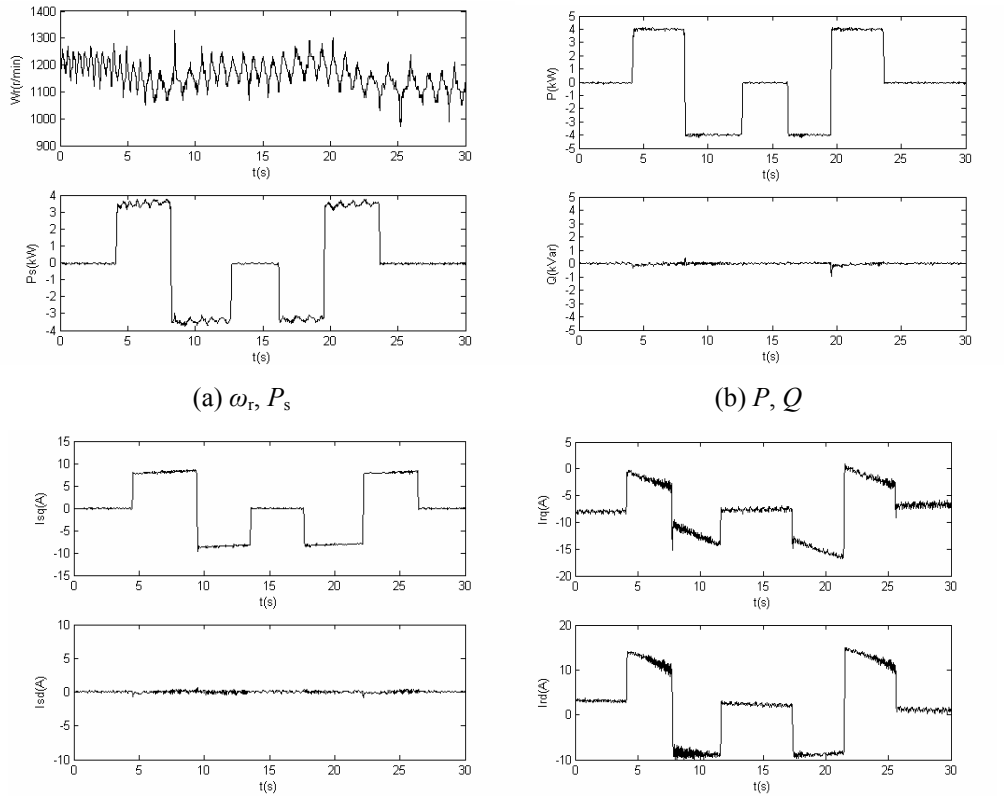

(a) ω_r, P_s (b) P, Q

(c) I_{sq}, I_{sd} (d) I_{rq}, I_{rd}

Fig. 13. Test results of the FPC prototype on P regulation at super-synchronous

5.3 Super-Synchronous

The prototype is tested on the power regulation at super-synchronous. P_{ref} and Q_{ref} can be set at any value within the working range of P and Q. Figs. 13–15 show the test results of the prototype on the power regulation at super-synchronous

When the prototype is tested on P and Q regulations at super-synchronous, the order variations of the P_{ref} and Q_{ref} values are the same as those at sub-synchronous. Figs. 13–15 show the test results of the prototype on P and Q regulations at super-synchronous, respectively.

Figs. 13–14 show the curves of ω_r, P_s, P, Q, I_{sq}, I_{sd}, I_{rq}, and I_{rd} on P and Q regulations at super-synchronous, respectively. As shown in Figs. 13–14, the P and Q regulations of the prototype at super-synchronous are implemented satisfactorily. Satisfactory performances of P and Q are obtained. ω_r accelerates or decelerates with the positive or negative value of P. Due to its loss, ω_r also slows down when P is zero. The relationship between P and P_s is the same as shown in (13). During the power regulation at super-synchronous, the changes of I_{sq}, I_{sd}, I_{rq}, and I_{rd} are the same as those shown in (15)–(16). In Figs. 13–14, the power regulation at super-synchronous is implemented satisfactorily.

Fig. 15 shows the power dynamic response of the FPC prototype at super-synchronous. Fig. 15(a) and (b) show the P and Q responses at super-synchronous, respectively. In Fig. 15, the P ramp time from 4 kW to -4 kW is 70 ms; the P ramp time from -4 kW to 4 kW is 50 ms; and the Q ramp time from 4 kW to -4 kW and from -4 kW to 4 kW are both about 60 ms. The sensitive response of the power regulation at super-synchronous is obtained.

Based on the test results, the prototype meets the design requirement on power regulation and starting. The proposed control strategy is thus implemented satisfactorily. The prototype meets the requirements on the power dynamic response for improving the grid stability.

6. Conclusion

This paper proposes an FPC composed of a DFIM, a flywheel with very large rotating inertia, a voltage-source PWM rectifier-inverter pair that is connected between the rotor and the grid and used as an AC exciter, and a corresponding control system. By incorporating the flywheel energy storage and the DFIM, the proposed FPC can store energy as available, supply a large amount of active power as needed, and provide reactive power for voltage support as necessary.

The structure of the FPC is described in detail, including

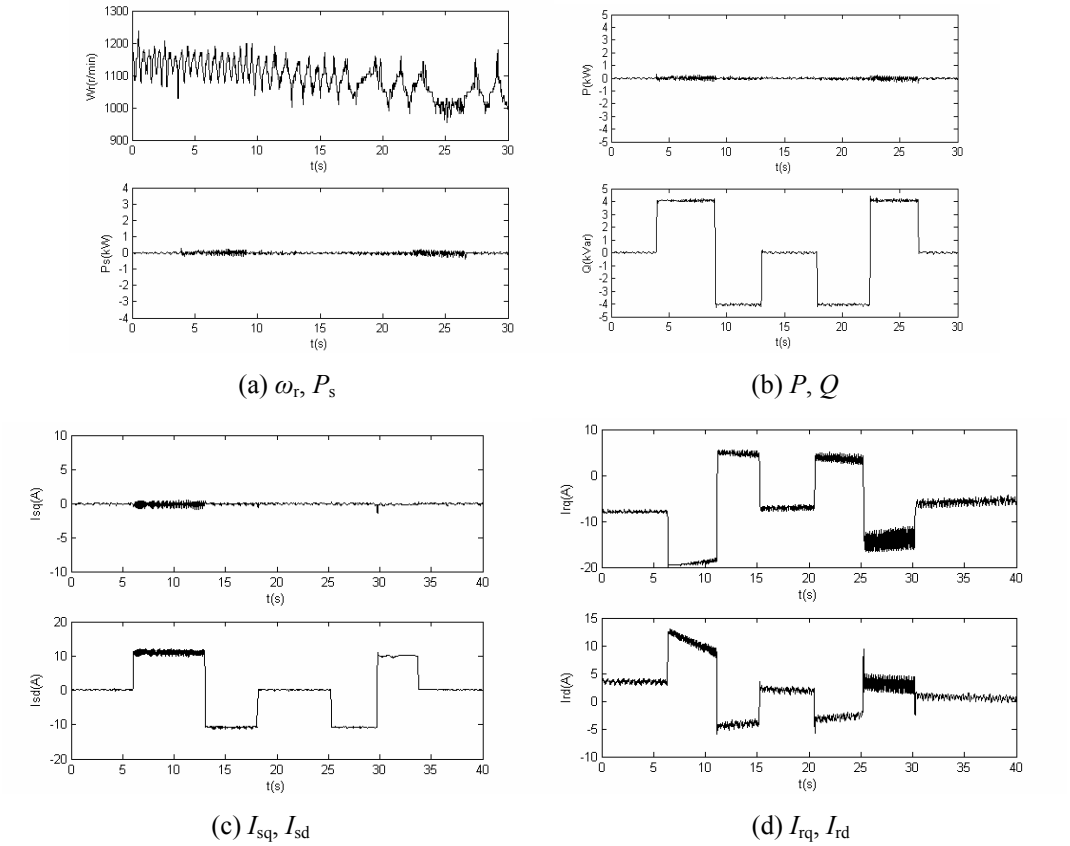

(a) ω_r, P_s (b) P, Q

(c) I_{sq}, I_{sd} (d) I_{rq}, I_{rd}

Fig. 14. Test results of the FPC prototype on Q regulation at super-synchronous

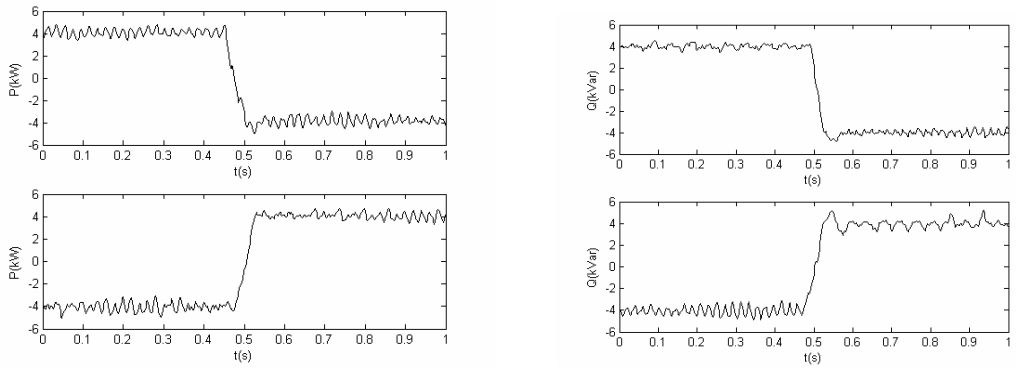

(a) P responses (b) Q responses

Fig. 15. Power dynamic response of the FPC prototype at super-synchronous

the flywheel and drive motor, and the converters. The control system of the FPC, which consists of three levels, namely, upper level controller, middle level controller, and bottom level controller, is investigated with an emphasis on the middle level controller. The SVOC technology is used for the design of the middle level controller, which determines the excitation voltage of the DFIM. The bottom level controller conducts the PWM-based excitation control for the machine, while the upper level controller performs a power or voltage control strategy at the power system level. The control strategy of the FPC direct start is also investigated in detail and the operating characteristics are analyzed. The simulation comparison of the FPC with the flywheel system, which uses the synchronous machine, is discussed as well as the operation modes of the FPC,. A prototype of the FPC is developed and tested at direct start, sub-synchronous, and super-synchronous.

Based on the test results, the prototype meets the design requirements on power regulation and starting. The proposed control strategy is thus implemented satisfactorily. The prototype meets the requirements on the power dynamic response for improving grid stability. Therefore,

the FPC provides a cost-effective and efficient means to improve power system stability by compensating for the unbalanced power using energy storage.

Acknowledgements

This work was supported by the National Natural Science Foundation of China (50937002), the Natural Science Foundation of Hubei Province in China (2009CDA042), and the National Basic Research Program of China (2009CB219702).

References

[1] A. Oudalov, D. Chartouni, and C. Ohler, "Optimizing a Battery Energy Storage System for Primary Frequency Control", IEEE Trans. Power Systems, 2007, 22, (3), pp. 1259–1266

[2] B. Singh, and G. K. Kasal, "Voltage and Frequency Controller for a Three-Phase Four-Wire Autonomous Wind Energy Conversion System", IEEE Trans. Energy Convers., 2008, 23, (2), pp. 509–518

[3] R. P. Torrico-Bascope, D. S. Oliveira, C. G. C. Branco, and F. L. M. Antunes, "A UPS With 110-V/220-V Input Voltage and High-Frequency Transformer Isolation", IEEE Trans. Ind. Electron., 2008, 55, (8), pp. 2984–2996

[4] K. Strunz, and H. Louie, "Cache Energy Control for Storage: Power System Integration and Education Based on Analogies Derived From Computer Engineering", IEEE Trans. Power Systems, 2009, 24, (1), pp. 12–19

[5] Md. H. Rahman, and S. Yamashiro, "Novel Distributed Power Generating System of PV-ECaSS Using Solar Energy Estimation", IEEE Trans. Energy Conversion., 2007, 22, (2), pp. 358–367

[6] S. Santoso, "On Determining the Relative Location of Switched Capacitor Banks", IEEE Trans. Power Del., 2007, 22, (2), pp. 1108–1116

[7] S. Santoso, and D. Hansen, "Practical Solutions for Broadband and Time-Varying Interharmonic Problems", IEEE Trans. Power Del., 2007, 22, (2), pp. 1228–1234

[8] Hailian Xie, L. Angquist, and H. P. Nee, "Investigation of StatComs With Capacitive Energy Storage for Reduction of Voltage Phase Jumps in Weak Networks", IEEE Trans. Power Systems, 2009, 24, (1), pp. 217–225

[9] R. Cardenas, R. Pena, G. M. Asher, J. Clare and R. Blasco-Gimenez, "Control strategies for power smoothing using a flywheel driven by a sensorless vector-controlled induction machine operating in a wide speed range", IEEE Trans. Ind. Electron., 2004, 51, (3), pp. 603–614

[10] G. O. Cimuca, C. Saudemont, B. Robyns, and M. M. Redulescu, "Control and performance evaluation of a flywheel energy-storage system associated to a variable-speed wind generator", IEEE Trans. Ind. Electron., 2006, 53, (4), pp. 1074–1085

[11] R. Cardenas, R. Pena, M. Perez, J. Clare, G. Asher and P. Wheeler, "Power smoothing using a flywheel driven by a switched reluctance machine", IEEE Trans. Ind. Electron., 2006, 53, (4), pp. 1086–1093

[12] S. M. Lukic, Jian Cao, R. C. Bansal, F. Rodriquez, and A. Emadi, "Energy storage systems for automotive applications", IEEE Trans. Ind. Electron., 2005, 55, (6), pp. 2258–2267

[13] B. H. Kenny, R. Jansen, P. Kascak, T. Dever, and W. Santiaqo, "Integrated power and attitude control with two flywheels", IEEE Trans. Aerospace and Electronic Systems, 2005, 41, (4), pp. 1431–1449

[14] M. L. Lazarewicz, and A. Rojas, "Grid frequency regulation by recycling electrical energy in flywheels", Power Engineering Society General Meeting 2004, June 2004, pp.2038–2042

[15] Haichang Liu, and Jihai Jiang, "Flywheel energy storage—An upswing technology for energy sustainability", Energy and Buildings, 2007, 39, (5), pp. 599–604

[16] H. Fujita, H. Akagi, M. Tan, and S. Ogasawara, "Occurrence and suppression of DC-flux deviations in a doubly-fed flywheel generator system", in Proc. IEEE 38th Industry Application Conference, Oct. 2003, pp. 1766–1771

[17] R. Datta, and V. T. Ranganathan, "A method of tracking the peak power points for a variable speed wind energy conversion system", IEEE Trans. Energy Convers., 2003, 18, (1), pp. 163–168

[18] J. W. Park, K. W. Lee, and H. J. Lee, "Control of active power in a doubly-fed induction generator taking into account the rotor side apparent power", in Proc. IEEE 35th Power Electronics Specialists Conference, June 2004, pp. 2060–2064

[19] H. Akagi, and H. Sato, "Control and performance of a doubly-fed induction machine intended for a flywheel energy storage system", IEEE Trans. Power Electronics, 2002, 17, (1), pp.109–116

[20] Yifan Tang, and Longya Xu, "Vector control and fuzzy logic control of doubly fed variable speed drives with DSP implementation", IEEE Trans. Energy Convers., 1995, 10, (4), pp.661–668

[21] A. Tapia, G. Tapia, J. X. Ostolaza, and J. R. Sanenz, "Modeling and control of a wind turbine driven doubly fed induction generator", IEEE Trans. Energy Convers., 2003, 18, (2), pp.194–204

[22] Gang Li, Jing Zhang, Shijie Cheng, Jinyu Wen, and Yuan Pan, "Space Formulation and Stability Analysis of a Doubly-fed Induction Machine with a Flywheel Energy Storage System", in Proc. PowerCon 2006., 2006.

[23] Gang Li, Shijie Cheng, Jinyu Wen, Yuan Pan, and Jin Ma, "Power system stability enhancement by a double-fed induction machine with a flywheel energy storage system", IEEE Power Engineering Society General Meeting 2006, 2006.
[24] H. Akagi, "Large static converters for industry and utility applications", Proceedings of the IEEE, 2001, pp. 976–983
[25] R. Pena, J. C. Clare, and G. M. Asher, "Doubly fed induction generator using back-to-back PWM converters and its application to variable-speed wind-energy generation", in Proc. IEE. Electric Power Applications, May 1996, pp.231–241
[26] R. G. de Almeida, J. A. P. Lopes, and J. A. L. Barreiros, "Improving power system dynamic behavior through doubly fed induction machines controlled by static converter using fuzzy control", IEEE Trans. Power Systems, 2004, 19, (4), pp.1942–1950
[27] G. Abad, M. A. Rodriquez, and J. Poza, "Three-level NPC converter-based predictive direct power control of the doubly fed induction machine at low constant switching frequency", IEEE Trans. Ind. Electron., 2008, 55, (12), pp. 4417–4429
[28] J. M. Mauricio, A. E. Leon, A. Gomez-Exposito and J. A. Solsona, "An adaptive nonlinear controller for DFIM-based wind energy conversion systems", IEEE Trans. Energy Convers., 2008, 23, (4), pp. 1025–1035
[29] D. Aouzellaga, K. Ghedamsia, and E. M. Berkouk, "Network power flux control of a wind generator", Renewable Energy, 2009, 34, (3), pp. 615–622

Appendix

The parameters of the FPC prototype used are given below:

Rated power P_N =4 kW, Stator rated voltage U_{sN}=380 V, Frequency f=50 Hz, Number of pole pairs p=3, Synchronous speed n_1=1000 rpm, Rated speed n_N =976.2 rpm, Range of slip -0.5<s<0.5, Rated power factor φ_N=0.816, Stator resistance R_s =1.5818 Ω, Rotor resistance Rr=1.4797 Ω, Stator inductance $L_{s\sigma}$=0.00855 H, Mutual inductance L_m=0.31395 H, Moment of inertia J=19 kg.m^2.

Jinbo Wu was born in Changsha, China in 1981. He received his B.S. degree from Hunan University (HNU), China in 2004, and his Master of Engineering Degree from Guangxi University (GXU), China in 2007. He is currently conducting research on the design of the practical device and control strategy of a doubly-fed induction machine with a flywheel energy storage system (FPC, Flexible Power Conditioner) toward obtaining his Ph.D. degree at Huazhong University of Science and Technology (HUST).

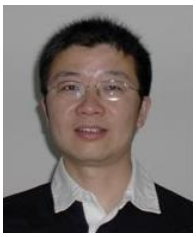

Jinyu Wen received his B.Eng. and Ph.D. degrees in electrical engineering from Huazhong University of Science and Technology (HUST), Wuhan, China, in 1992 and 1998, respectively. He was a visiting student from 1996 to 1997, and research scholar from 2002 to 2003 at the University of Liverpool, UK. In 2003, he joined the HUST, where he presently serves as professor. He is a visiting research fellow at the University of Texas at Arlington, USA. His current research interests include smart grid, renewable energy, energy storage, FACTS, HVDC, and power system operation and control.

Haishun Sun obtained his B.S., M.S., and Ph.D. degrees from Huazhong University of Science and Technology (HUST) in 1991, 1997, and 2004, respectively. He is an associate professor at HUST. His research interests include power system analysis, distributed generation, and shipboard power system.

Shijie Cheng graduated from the Xi'an Jiaotong University, Xi'an, China in 1967 and received his Master of Engineering Degree from the HUST, Wuhan, China in 1981. He earned his Ph.D. from the University of Calgary, Calgary, Canada in 1986. All three degrees are in the field of Electrical Engineering. He is now a full professor at the HUST. His research interests are power system control, stability analysis of power system, and application of Al in power systems.